

RESEARCH ARTICLE

A self-consistent model of helium in the thermosphere

10.1002/2015JA021223

Key Points:

- TIE-GCM has been modified to account for neutral helium
- Seasonal behavior is successfully captured
- Neutral densities from the new model agree well with previous observations

Supporting Information:

- Supporting Information S1
- Movie S1
- Figure S1
- Figure S2
- Figure S3
- Figure S4

Correspondence to:

E. K. Sutton,
eric.k.sutton@gmail.com

Citation:

Sutton, E. K., J. P. Thayer, W. Wang, S. C. Solomon, X. Liu, and B. T. Foster (2015), A self-consistent model of helium in the thermosphere, *J. Geophys. Res. Space Physics*, 120, doi:10.1002/2015JA021223.

Received 18 MAR 2015

Accepted 17 JUL 2015

Accepted article online 20 JUL 2015

Eric K. Sutton¹, Jeffrey P. Thayer², Wenbin Wang³, Stanley C. Solomon³, Xianjing Liu^{2,4}, and Benjamin T. Foster³

¹Space Environment Branch, Air Force Research Laboratory, Albuquerque, New Mexico, USA, ²Aerospace Engineering Sciences Department, University of Colorado, Boulder, Colorado, USA, ³High Altitude Observatory, National Center for Atmospheric Research, Boulder, Colorado, USA, ⁴Now at Department of Atmosphere, Oceanic and Space Sciences, University of Michigan, Ann Arbor, Michigan, USA

Abstract We have found that consideration of neutral helium as a major species leads to a more complete physics-based modeling description of the Earth's upper thermosphere. An augmented version of the composition equation employed by the Thermosphere-Ionosphere-Electrodynamics General Circulation Model (TIE-GCM) is presented, enabling the inclusion of helium as the fourth major neutral constituent. Exospheric transport acting above the upper boundary of the model is considered, further improving the local time and latitudinal distributions of helium. The new model successfully simulates a previously observed phenomenon known as the "winter helium bulge," yielding behavior very similar to that of an empirical model based on mass spectrometer observations. This inclusion has direct consequence on the study of atmospheric drag for low-Earth-orbiting satellites, as well as potential implications on exospheric and topside ionospheric research.

1. Introduction

The presence of helium as a major component in the Earth's upper thermosphere and lower exosphere was first inferred from measurements of satellite drag. By analyzing orbital variations of the Echo 1 satellite orbiting above 1000 km, Nicolet [1961] reasoned that atomic oxygen was incapable of producing the observed satellite deceleration given reasonable values of exospheric temperature. Likewise, atomic hydrogen concentrations were thought to be much too low to create such a deceleration.

Increasingly direct evidence of helium's presence soon emerged from in situ mass spectrometer measurements taken onboard Explorer 17 [Reber and Nicolet, 1965]. Concomitant with this confirmation was the hint of a significant seasonal-latitudinal variation in the helium distribution, relative to the other measured constituents (i.e., molecular nitrogen and atomic oxygen). Soon thereafter, strong semiannual variations inferred from the satellite drag acting on Echo 2 [Cook, 1967] around 1100 km were linked to seasonal variations of helium concentration. Keating and Prior [1968] confirmed this result with satellite drag data from the Explorer 9, 19, and 24 satellites. They also noted an apparent enhancement near the winter pole, which they termed the "winter helium bulge," with an approximate winter-to-summer ratio of 2.5. Subsequent drag-inferred calculations by Keating *et al.* [1970] yielded ratios in excess of 3 at an altitude of 850 km.

Reber *et al.* [1971], using mass spectrometer measurements from the Ogo 6 satellite, showed an order-of-magnitude difference between the helium content in winter and summer hemispheres near 400–600 km altitude. This disagreement with previous results highlighted the limitations of the drag-inferred technique, specifically, reliance on the assumption of diffusive equilibrium to separate composition-induced mass density variations from those caused by temperature. In response, Keating *et al.* [1974] augmented their drag-inferred technique to include a description of the background composition that was consistent with the available mass spectrometer data. New ratios in excess of an order of magnitude could then be obtained through this method as well. In addition to establishing a larger bulge ratio, Reber *et al.* [1971] noted a strong correlation of the maximum helium density with the location of the winter geomagnetic pole. This was interpreted as a sensitivity of the helium distribution to the thermospheric wind system.

In addition to high-latitude variations near the solstices, Newton *et al.* [1973] detected a strong local time preference for helium concentration as measured by mass spectrometers on the low-inclination San Marco 3 satellite. Reber *et al.* [1973] and Mayr *et al.* [1974] discussed similar variations manifest within the Ogo 6 density

model [Hedin *et al.*, 1974]. These findings showed a preference of the diurnal maxima toward earlier times for species with small molecular masses, the opposite being true for species with large masses. The San Marco 3 observations, taken at altitudes near 225 km, showed a preference toward the 06–09 LT sector while those taken by Ogo 6, near 450 km, showed maxima closer to 10 LT.

The realization of these phenomena motivated several modeling studies to uncover the mechanism responsible for the counterintuitive distribution of helium in the thermosphere. Noticing that helium vertical profiles measured by several rocket-based mass spectrometers departed quite drastically from diffusive equilibrium, an early study by Kasprzak [1969] invoked an additional diffusive flux in order to reconcile the observations with his model. This treatment required vertical fluxes on the order of 6×10^8 and $2 \times 10^{10} \text{cm}^{-2} \text{s}^{-1}$ for summer and winter conditions, respectively, over an altitude range of 120–200 km. Kockarts [1973] later noted, however, that these values were larger than the maximum flux allowed by molecular diffusion, thus requiring an additional mechanism of transport.

Johnson and Gottlieb [1970] used basic considerations of continuity to show that a general summer-to-winter flow of the major atmospheric constituents could account for a buildup of helium in the winter polar regions. Without discounting these findings, several attempts were made to ascertain the effect of atmospheric fluctuations on helium transport. Hodges [1970] modeled large-scale fluctuations as monochromatic plane waves, which effected a downward transport and an overall decrease to the scale height of species with masses smaller than the mean mass. Similarly, Kockarts [1972] derived the eddy diffusivity profile necessary to reconstruct the winter helium bulge observations of Reber *et al.* [1971], under the assumption of molecular diffusion in the absence of wind. Results from these studies suggested that eddy diffusion could in fact control the global helium distribution. However, recreating the observed winter bulge ratios required more than an order-of-magnitude increase in eddy diffusivity from winter to summer hemispheres. These results were qualitatively consistent with each other, yet they implied that similar latitudinal signatures should be evident in other minor atmospheric constituents, a feature that was inconsistent with previous observations of atomic oxygen [Kockarts, 1973].

Reber and Hays [1973] performed a more rigorous treatment of the effects of circulation on the distribution of helium. Included in their model were the effects of molecular and eddy diffusion as well as a parameterized circulation pattern of the background gas that satisfied continuity requirements and could be tuned to simulate a given level of summer-to-winter flow. Combining the equations of continuity and momentum for a minor species led to an accurate representation of previous winter helium bulge observations. The idea that the winter helium bulge could be completely explained by seasonal circulation patterns led, however, to an apparent paradox. At times of high solar flux, when an enhanced summer-to-winter flow had been expected to occur, smaller pole-to-pole helium ratios had been observed. Reber and Hays [1973] explained the discrepancy by invoking the mechanism of exospheric flow, whereby during times of high solar flux, increased temperatures in the upper thermosphere drive a larger exospheric flow directed away from the winter bulge. The balance between the circulation-induced effects and exospheric transport was found to control the magnitude of the latitudinal gradient in helium concentration that could be supported by the atmosphere.

By analyzing the combined equations of continuity and momentum for a minor species, Reber and Hays [1973] and Hays *et al.* [1973] identified the vertical advection term as being responsible for establishing the seasonal distribution of helium. In the presence of diffusively separated atmospheric constituents, this term leads to increased helium densities in regions of downwelling and decreased densities in regions of upwelling. The opposite behavior is implied for species, such as argon, that are heavier than the local mean mass. Reber [1976] further explained that in order to perturb composition from the distribution prescribed under conditions of diffusive equilibrium, the vertical winds must be significant in relation to a characteristic vertical diffusive velocity, $v_D = D/H$, where D is the mutual diffusion coefficient and H is the atmospheric scale height.

Contemporaneous works by Mayr and Volland [1972, 1973] asserted a similar yet distinct perspective on the matter. Mayr *et al.* [1978] summarized these findings and coined the phrase “wind-induced diffusion,” describing horizontal transport in the presence of diffusively separated constituents. Both groups agreed that the interaction between helium and the background circulation—consisting of upwelling in the summer hemisphere, summer-to-winter flow, and downwelling in the winter hemisphere—would lead to a winter helium bulge consistent with observations. However, Reber and Hays [1973] suggested that the transport mechanism was related to the vertical advective motion in the presence of diffusive separation, while Mayr *et al.* [1978] believed horizontal bulk motion in the presence of diffusive separation to be responsible.

As the basic mechanism causing the observed helium behavior—i.e., circulation within a diffusively separated atmosphere—continued to mature, several successful satellite mass spectrometer missions served to refine these theories and document the phenomenological implications. The open-source mass spectrometers on Atmospheric Explorer satellites (AE-C, AE-D, and AE-E) were used by several investigators to further quantify seasonal variations [Mauersberger *et al.*, 1976a, 1976b; Cageao and Kerr, 1984]. Reber *et al.* [1975] also analyzed these data to study waves in composition, showing coherent phase relationships between the various constituents. Hedin and Carignan [1985] used data from the Dynamics Explorer 2 (DE-2) satellite to show that even during geomagnetically quiet times, signatures of helium depletion are present near the magnetic poles. These data sets now comprise the majority of our understanding of thermospheric composition, the empirical basis of which is embodied by the Mass Spectrometer and Incoherent Scatter (MSIS) series of models [Hedin, 1987, 1991; Picone *et al.*, 2002], successors of the Ogo 6 model. More recently, Thayer *et al.* [2012] inferred strong signatures of helium from differences in total mass densities measured at two different altitudes by high-precision accelerometers on board the Challenging Mini-Satellite Payload and Gravity Recovery and Climate Experiment satellites [Sutton, 2011]. Liu *et al.* [2014a] extended this work, showing that the response of the mass density vertical profile during a geomagnetic disturbance is quite sensitive to the atomic oxygen/helium transition height.

The remainder of this paper is organized as follows. Section 2 introduces a self-consistent method for calculating helium abundances and transport by modifying an existing general circulation model of the thermosphere. Unlike previous formulations, we do not impose the assumption that helium remains a minor species throughout the model domain, which can have deleterious effects at high altitudes. Section 3 highlights the salient features of the new model, including helium's role in determining mean mass, total mass density, pressure level height, and winds.

2. Model Description

2.1. TIE-GCM

The model developments described in this paper have been applied to the National Center for Atmospheric Research Thermosphere-Ionosphere-Electrodynamics General Circulation model (NCAR/TIE-GCM) v.1.95 [Roble *et al.*, 1988; Richmond *et al.*, 1992] and are slated for inclusion in the next TIE-GCM and TIME-GCM [Roble and Ridley, 1994] model versions. The TIE-GCM is a first-principles upper atmospheric general circulation model that solves the Eulerian continuity, momentum, energy, and composition equations for the coupled thermosphere-ionosphere system. The vertical coordinate is specified by log pressure levels in half-scale height increments, providing coverage in altitude of approximately 97 km to 600 km, the latter being dependent on solar activity.

Tidal forcing at the lower boundary is specified by the Global Scale Wave Model [Hagan *et al.*, 2001]. Annual and semiannual variations in subgrid turbulent fluctuations are taken into account by applying seasonal variation of the eddy diffusivity coefficient at the lower boundary [Qian *et al.*, 2009, 2013]. Based on measurements from the Mauna Loa Observatory [Keeling and Whorf, 2005], the mixing ratio of CO₂ imposed at the lower boundary was set to 364 ppmv for 1996, increasing linearly by 1.5 ppmv per year thereafter.

In the simulations presented throughout this paper, solar irradiance is specified in a manner consistent with Solomon *et al.* [2011]. The $M_{10.7}$ index is used in place of the $F_{10.7}$ solar proxy in an effort to better capture solar UV and EUV irradiance during the deep solar minimum of 2008. The $M_{10.7}$ index derives from the magnesium core-to-wing ratio (MgII c/w) of Viereck *et al.* [2004] via a linear fit to the $F_{10.7}$ proxy calculated during 1978–2007 [Solomon *et al.*, 2011]. With this normalization, $M_{10.7}$ can be used in place of $F_{10.7}$ to drive the EUVAC proxy model [see Richards *et al.*, 1994; Woods and Rottman, 2002; Solomon and Qian, 2005].

Magnetospheric inputs to the polar regions are specified by an applied electric potential pattern and an auroral precipitation oval. The Heelis *et al.* [1982] empirical specification of magnetospheric potential in the ionosphere, which is parameterized by the 3 h geomagnetic K_p index, is the standard TIE-GCM input and is employed for the simulations presented throughout this paper. Auroral precipitation is applied as described by Roble and Ridley [1987] based on the estimated hemispheric power of precipitating electrons. The empirical estimate of this power as it depends on K_p has been increased from its original formulation by a factor of ~ 2 , based on results from the Global Ultraviolet Imager on the TIMED satellite [Zhang and Paxton, 2008].

The TIE-GCM uses the method outlined by Richmond *et al.* [1992] to calculate the low-latitude ionospheric electrodynamic driven by conductances and neutral dynamics. The calculated electric potential is merged

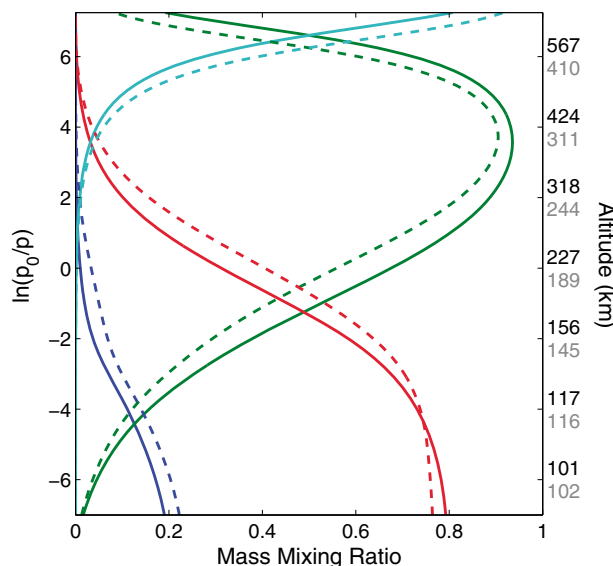


Figure 1. MSIS mass mixing ratios for O₂ (blue), O (green), N₂ (red), and He (cyan) calculated on the vertical log pressure scale in the vicinity of the winter helium bulge for solar maximum (solid lines/black altitude labels, 21 Dec. 2000) and minimum (dashed lines/grey altitude labels, 21 Dec. 2008) conditions.

with the externally imposed potential within each polar cap, using crossover boundaries that vary dynamically with the size of the magnetospheric potential pattern. See *Solomon et al.* [2012, section 2.3] for further detail concerning the high-latitude inputs and *Solomon et al.* [2011, section 4] for a discussion of model uncertainties.

2.2. Helium as a Major Species

The equations describing the transport and concentration of the various components in the upper atmosphere are coupled to one another through diffusive and chemical processes. When solving for the concentration of a minor species [Roble et al., 1988], several terms in the fully coupled composition equation are assumed to be small. With the neglect of these terms, the solution of the major species composition becomes dynamically decoupled from that of the minor species composition, leading to a more efficient segmented numerical solution.

The main terms that must be neglected are those in the diffusion matrix describing the acceleration experienced by any major species caused by collisions with the minor species as well as those that account for the effect that the minor species has on the mean mass and scale height of the atmosphere. It is straightforward to show that the effect of these terms is small when the mass mixing ratio of the minor species in question is also small. Helium as a minor species in the TIE-GCM was recently implemented by *Liu et al.* [2014b]. While this approach demonstrated the model's ability to accumulate helium in the winter hemisphere, it required the ad hoc inclusion of helium into the scale height calculation in order to avoid unrealistically high values during long simulations.

As a simple test, an empirical approach can be used to ascertain whether or not helium satisfies the assumptions necessary to treat it as a minor constituent. We employ the MSIS model [Picone et al., 2002], which represents helium abundance in an averaged sense as observed by mass spectrometer observations spanning several decades. However, care must be taken when converting between the vertical coordinate systems of MSIS and TIE-GCM. The TIE-GCM uses log pressure, $z = \ln(p_0/p)$, as its vertical coordinate, where p_0 is a reference pressure set to $5 \times 10^{-4} \text{ g}/(\text{cm} \cdot \text{s}^2)$. In order to obtain a reasonable estimate of the amount of helium that should be present within the vertical domain of the TIE-GCM, it is necessary to compute MSIS densities with respect to the TIE-GCM's log pressure scale. Using the ideal gas law, we directly calculate the log pressure level from the number densities and temperatures specified by MSIS.

As molecular diffusion becomes dominant with increasing height, a neutral species of comparatively small mass such as helium will increase in relative concentration. Due to the interaction between global circulation and molecular diffusive flow, the largest values tend to occur at high latitudes in the winter hemisphere [e.g., Reber and Hays, 1973; Mayr et al., 1978]. Figure 1 shows that under these conditions and near the top level of the TIE-GCM (i.e., roughly 500–700 km, depending on solar flux), helium mass mixing ratios exceed 0.8 during solar maximum conditions and 0.9 during solar minimum conditions. Had we instead queried MSIS using the geometric heights calculated by TIE-GCM as our vertical coordinate, values just below 0.5 would have been obtained. As will be shown in section 3, this discrepancy stems from an underestimation of the geometric height in the upper thermosphere by the original TIE-GCM code due to the neglect of helium. In either case, empirical evidence suggests that helium becomes a major neutral component—and perhaps the dominant component—under certain conditions within the spatial domain of the TIE-GCM. In light of these findings, the remainder of this section covers the expansion of the major neutral species composition equation and

Table 1. Mutual Diffusion Coefficients for Helium With Major Species^a

| $i-j$ | a | s |
|-------------------|-------|-------|
| He-O ₂ | 0.649 | 1.710 |
| He-O | 0.866 | 1.749 |
| He-N ₂ | 0.622 | 1.718 |

^a $D_{ij} = a(T/T_{00})^s(p_{00}/p)$, $T_{00} = 273\text{K}$, $p_{00} = 10^6\text{g}/(\text{cm} \cdot \text{s}^2)$ [cf. *Banks and Kockarts, 1973, Table 15.1*].

other modeled processes from a three-constituent description [*Dickinson et al., 1984*] to a four-constituent description in order to account for the significant effects of helium.

The evolution of the major neutral species composition can be expressed using the following vector equation (see the Appendix for derivation and a complete definition of variables):

$$\frac{\partial \Psi}{\partial t} = -e^z \tau^{-1} \frac{\partial}{\partial z} \left[\frac{\bar{m}}{m_{\text{N}_2}} \left(\frac{T_{00}}{T} \right)^{0.25} \alpha^{-1} \mathbf{L} \Psi \right] + e^z \frac{\partial}{\partial z} \left[e^{-z} K_E(z) \left(\frac{\partial}{\partial z} + \frac{1}{\bar{m}} \frac{\partial \bar{m}}{\partial z} \right) \Psi \right] - (\mathbf{V} \cdot \nabla \Psi + \omega \frac{\partial \Psi}{\partial z}) + \mathbf{s} \quad (1)$$

The meanings of several variables have been modified from those originally intended by *Dickinson et al.* [1984]. Ψ is now the vector of mass mixing ratios for O₂, O, and He, while the mass mixing ratio of the remaining major constituent N₂ is specified by $\psi_{\text{N}_2} = 1 - \psi_{\text{O}_2} - \psi_{\text{O}} - \psi_{\text{He}}$. Molecular and thermal diffusion are accounted for by the first term on the right side of equation (1), eddy diffusion by the second, horizontal and vertical advection by the third, and chemical sources and sinks by the fourth.

\mathbf{L} is a diagonal matrix operator with elements

$$L_{ii} = \frac{\partial}{\partial z} - \left(1 - \frac{m_i}{\bar{m}} - \frac{1}{\bar{m}} \frac{\partial \bar{m}}{\partial z} - \frac{\alpha_{Ti}}{T} \frac{\partial T}{\partial z} \right) \quad (2)$$

which have been expanded to describe thermal diffusion, a phenomenon which becomes important for species such as helium whose masses are quite different from the mean mass. We use a simplified formulation of thermal diffusion that is analogous to its appearance in the binary diffusion equations, after *Colegrove et al.* [1966]. In this treatment, a constant value of $\alpha_{\text{He}} = -0.38$ is used. While this value is characteristic of small concentrations of helium diffusing through molecular nitrogen, this assumption is reasonably accurate at altitudes where significant temperature gradients exist (i.e., below ~ 200 km) [*Banks and Kockarts, 1973*].

The normalized molecular diffusion matrix, α , couples the major components to one another. As can be seen in equations (A18) and (A23) in the Appendix, the strength of this coupling depends on the mutual diffusion coefficients. *Dickinson et al.* [1984] assumed these coefficients to take the form $D = D_0(T/T_{00})^{1.75}(p_{00}/p)$ for the major species, after *Colegrove et al.* [1966]. Accordingly, the elements of α have been normalized by this functional form. Mutual diffusion coefficients between helium and the other three major species take a similar form, yet with exponents, s , that deviate slightly from 1.75, as seen in Table (1). These differences have been accounted for by applying correction factors of the form $(T/T_{00})^{1.75-s}$ to the appropriate terms within the diffusion matrix α . In the absence of these corrections, the coefficient describing the mutual diffusion between helium and atomic oxygen would remain reasonably accurate, yet those describing the interaction of helium with molecular species would be approximately 5% low.

The chemical source and sink matrix, \mathbf{s} , also serves to couple the major species to one another. In the case of helium, however, all chemical and photochemical rates have been set to zero, consistent with our assumption of inertness. Therefore, our current model implementation is appropriate for the study of the dynamical behavior of helium as an ideal inert tracer.

The neutral thermodynamic properties of specific heat, c_p , molecular viscosity, k_m , and conductivity, k_t , have been augmented to include the effects of helium. The following equations are now used [*Banks and Kockarts, 1973*]:

$$c_p = \frac{R}{2n} \left(\frac{7}{32} n_{\text{O}_2} + \frac{5}{16} n_{\text{O}} + \frac{7}{28} n_{\text{N}_2} + \frac{5}{4} n_{\text{He}} \right) \text{erg} \cdot \text{g}^{-1} \text{K}^{-1} \quad (3)$$

$$k_m = \frac{10^{-6} T^{0.69}}{n} (4.03 n_{\text{O}_2} + 3.90 n_{\text{O}} + 3.43 n_{\text{N}_2} + 3.84 n_{\text{He}}) \text{g} \cdot \text{cm}^{-1} \text{s}^{-1} \quad (4)$$

$$k_t = \frac{T^{0.69}}{n} (56.0(n_{\text{O}_2} + n_{\text{N}_2}) + 75.9 n_{\text{O}} + 299.0 n_{\text{He}}) \text{erg} \cdot \text{cm}^{-1} \text{s}^{-1} \text{K}^{-1} \quad (5)$$

where R is the universal gas constant, T is the neutral temperature in units of Kelvin, n_i refers to the number density of the subscripted species, and n is the total number density.

Additionally, in the description of ambipolar diffusion, the collision frequency, ν_{in} , has been updated to account for nonresonant collisions between O^+ ions and neutral helium atoms. The following form is adopted [Schunk and Nagy, 2004]:

$$\nu_{in} = 1 \times 10^{-10} \left(6.64 n_{O_2} + 0.367 n_O \sqrt{T_r} (1 - 0.064 \log_{10} T_r) + 6.82 n_{N_2} + 1.32 n_{He} \right) \quad (6)$$

where $T_r = (T_i + T)/2$ is the average of the ion and neutral temperatures. T_r , ν_{in} , and n_i are in units of Kelvin, s^{-1} and cm^{-3} , respectively.

2.3. Boundary Conditions

At the lower boundary of the model, atomic and molecular oxygen adhere to the conditions specified in the original TIE-GCM implementation, namely, that the peak of the atomic oxygen density profile lies at the lower boundary and the total amount of oxygen atoms remains constant, making up 23.4% of the total mass. In addition, we specify a constant lower boundary mass mixing ratio for helium of 1.154×10^{-6} . In terms of mass mixing ratios, these considerations take the following form: (1) $\partial \psi_O / \partial z = \psi_O$, (2) $\psi_{O_2} + \psi_O = 0.234$, and (3) $\psi_{He} = 1.154 \times 10^{-6}$.

Near the upper boundary of the model, either atomic oxygen or helium typically dominates the composition, depending on season, solar flux, and location. The original upper boundary of the TIE-GCM is specified by diffusive equilibrium for neutral species, i.e., $\mathbf{L}\Psi = 0$. However, the large thermal velocity of helium warrants proper consideration of helium transport processes occurring above the upper boundary in a near-collisionless environment. While the classical thermal escape flux of helium is several orders of magnitude too low to have a noticeable effect on the global helium content, the lateral transport of helium atoms with ballistic trajectories is significant. Hodges and Johnson [1968] and Hodges [1973] outline a method for approximating this type of transport, expressing it as a vertical outward particle flux:

$$\Phi = -\nabla^2 (n \bar{v} H^2 P) \quad (7)$$

where ∇^2 is the surface Laplacian. The variables Φ , n , \bar{v} , and H are respectively the vertical particle flux, number density, mean thermal speed, and scale height, all specific to helium. P , a dimensionless factor arising from integration over Maxwellian distributions, has a weak dependence on neutral temperature that can be adequately approximated by [Hodges and Johnson, 1968]

$$P \approx \left(1 + \frac{T}{3300} \right) \quad (8)$$

for neutral temperature, T , in units of Kelvin. Inherent in these equations is the assumption that collisions do not occur above the upper boundary of the TIE-GCM.

In practice, this vertical flux can be prescribed at the upper boundary of the model as a diffusive flow. The following vector equation describing molecular diffusion is used:

$$\mathbf{w}_D = \tau^{-1} \left(\frac{T_{00}}{T} \right)^{0.25} \frac{p_0 \bar{m}}{g m_{N_2}} \alpha^{-1} \mathbf{L}\Psi \quad (9)$$

where \mathbf{w}_D is the (3×1) vector of vertical diffusive mass flow rates for O_2 , O , and He , respectively. From the derivation of equation (9) in the Appendix (see equation (A25)), it follows that the diffusive mass fluxes of all neutral species sum to zero. Because molecular oxygen and nitrogen densities are small near the upper boundary, we enforce this constraint by assuming that any outward (inward) mass flux of helium is balanced by an inward (outward) flux of atomic oxygen. Any error that this assumption incurs in the solution of atomic oxygen concentration is diminished by the factor of 4 difference between the mass of oxygen and helium atoms.

In the current implementation of our model, the argument of the Laplacian from equation (7) is transformed into a nonaliasing spherical harmonic expansion. This is completed using the technique of

Swarztrauber [1979], modified to accommodate the TIE-GCM's horizontal grid, which is offset from the pole by a half-grid increment. The flux, Φ , is then calculated using the well-known eigenfunction/eigenvalue relation:

$$\nabla^2 Y_n^m = -\frac{n(n+1)}{R^2} Y_n^m \quad (10)$$

where Y_n^m refers to the spherical harmonic function of degree n and order m and R is a characteristic radius of the exobase. In the current implementation, R has been set to the radius of the Earth for consistency with calculations of other horizontal derivatives within the TIE-GCM. The mass flux required by the left-hand side of equation (9) can then be obtained by transforming back to the spherical grid and multiplying the obtained particle flux by the molecular mass of helium. The advantage of using this technique in place of finite differences for calculating the Laplacian is that waves are resolved uniformly over the Earth. Therefore, the growth of numerical instabilities can be controlled by truncating the expansion prior to transforming back to the spherical grid. We note that the degree of truncation required is sensitive to the level of the upper boundary, the grid size, and the time step. When using the default $5^\circ \times 5^\circ \times H/2$ spatial grid with an upper boundary of $z = +7$ and a 120 s time step, we have found that a triangular truncation of degrees higher than 4 is sufficient to limit the growth of numerical instabilities without severely compromising the accuracy of the exospheric transport model. The adjustment of this truncation parameter, as well as the characteristic exobase radius, R , are left as tasks for future work.

3. Global Features

In this section, we present the salient features of the new model. While many simulations were necessary in order to distill our description of these features with respect to season, local time, latitude, external forcing parameters, and boundary conditions, only a small subset of simulations is presented. These were created using the model settings and inputs described in section 2.1 and are specific to the prevailing solar and geophysical conditions of 2008. The supporting information includes additional plots and an animation to aid in visualization, specifically regarding the sensitivity of the helium distribution to external forcing and boundary conditions.

Figure 2 shows helium densities at 250 km altitude simulated by the TIE-GCM during each of the four seasons of 2008. The winter helium bulge phenomenon is clearly present at both solstices. During the equinoxes, the helium bulge undergoes a migration from the spring hemisphere to the fall. Along the way, helium levels are briefly enhanced at low latitudes with a strong preference for early morning local times, with the full transition taking approximately 1–2 months. At winter solstice, a similar preference for early morning is tempered by an aversion to the auroral zones, where pockets of divergence and upwelling lead to localized helium depletions. This balance manifests as a diurnal modulation of the winter helium bulge in latitude and local time. Symptoms of this behavior can be seen in the the upper right panel of Figure 2, where the southern hemisphere winter peak occurs around 16:00 LT. For reference, the geomagnetic poles are located at $82.4^\circ\text{N}/18:30$ LT and $74.5^\circ\text{S}/8:20$ LT in these plots. Movie S1 also captures this diurnal undulation and its relationship with the distribution of auroral heating during Southern Hemisphere winter. Constant solar and geomagnetic forcing parameters were used to create the 1 day looping animation.

The high-latitude helium distribution is further complicated by short-scale variations in geomagnetic heating. In general, helium densities tend to increase at low latitudes during periods of geomagnetic activity. The opposite is true in the polar region during solstice, as the high-latitude upwelling and divergence resulting from geomagnetic activity tend to lift heavy constituents while dispersing helium over a larger horizontal expanse.

The distribution of helium is highly sensitive to geomagnetic activity, the effects of which can be seen in the contrasting equinoctial helium distributions of Figure 2. The March equinox consists of enhanced low- and middle-latitude helium densities accompanied by depletions closer to the poles, all associated with a slight elevation in the level of geomagnetic activity over the previous 3 h period ($Kp = 2.0$) relative to the September equinox ($Kp = 0.3$). The same argument can be applied to the solstice plots of Figure 2, wherein the slightly disturbed ($Kp = 2.0$) June solstice helium distribution is shifted away from the winter pole in comparison to the undisturbed ($Kp = 0.0$) December solstice. The helium distribution is most certainly influenced by the time history of geomagnetic activity over the previous ~ 24 h or more. As such, an index describing the level of geomagnetic activity over a 3 h interval may not generally be a reliable indicator. However, in all four of

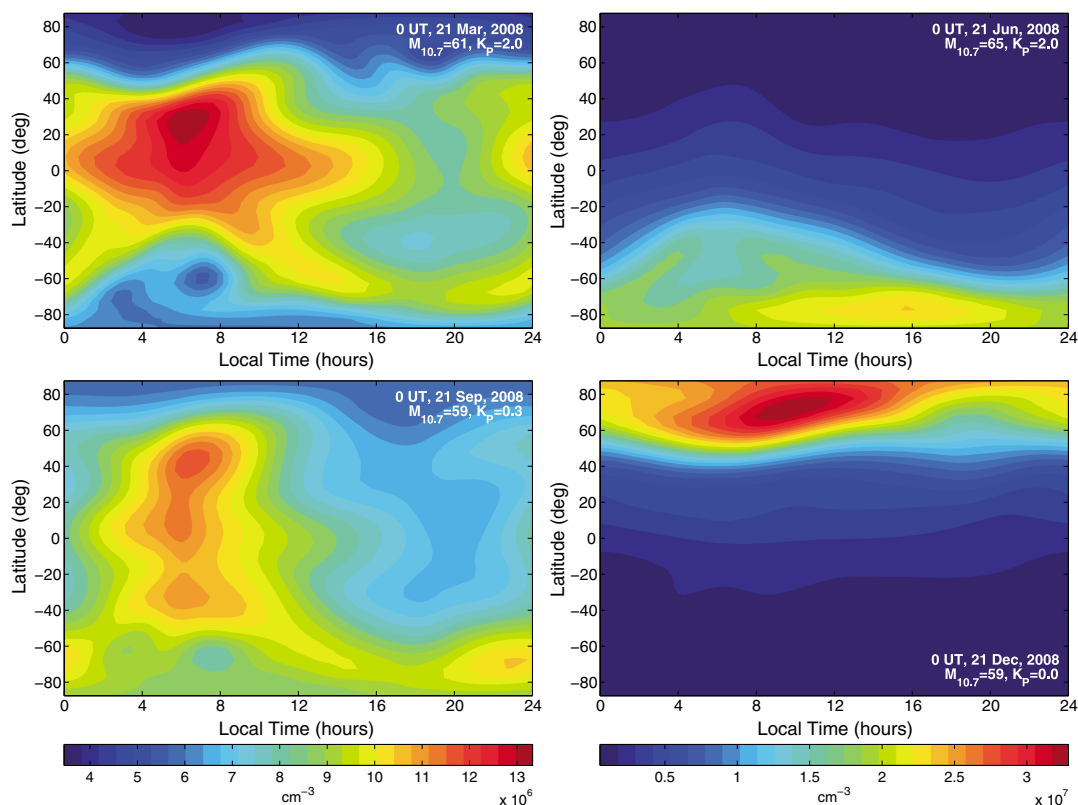


Figure 2. Global distribution of helium number densities at 250 km altitude during each season for solar minimum conditions (2008), as calculated by TIE-GCM. (left) Equinox plots share a common color scale, as do (right) solstice plots.

the cases presented, the 3 h K_p index is fairly representative of the levels of geomagnetic activity during the previous 24 h period. The solstice comparison is less straightforward than for equinox due to several additional complications. One such complication is that the location of maximum helium concentration is more sensitive during solstice to the location of the geomagnetic poles. The solstice comparisons also suffer from slightly differing amounts of solar flux. The supporting information provides additional figures emphasizing the sensitivity of the helium distribution throughout the year to variations in geomagnetic activity, solar flux, and forcing of the lower boundary by migrating tides.

As a basis for comparison, Figure 3 shows helium densities at 250 km altitude as calculated by the MSIS model. Many of the salient features are qualitatively similar to those of the TIE-GCM, with respect to seasonal, latitudinal, and local time characteristics. MSIS helium distributions clearly exhibit the same strong preference for the winter polar regions during solstice, and for the low-latitude, early local time sectors during equinox. Likewise, a similar sensitivity to geomagnetic effects is evident within MSIS. Notice, however, that the color scales differ between Figures 2 and 3 in order to show behavior over the full range of each model. At 250 km, the TIE-GCM typically underestimates the magnitude of the MSIS helium bulge by approximately 20% during solstice, while overestimating it by 5% during equinox. This agreement is reasonable, considering that no adjustments have been made to the TIE-GCM in an effort to improve model agreement. Likewise, the MSIS model estimated and applied correction factors for the underlying mass spectrometer data [Hedin, 1987], which could further limit the absolute accuracy of such model comparisons. In certain cases, there are discrepancies in the location and shape of the helium bulge between models. For instance, the location of maximum helium concentration during the June solstice is out of phase by about 8 h in local time between the two models. While the MSIS helium distribution is prescribed, to a certain extent, by a trade-off between the data sparsity of its underlying historical data set and the complexity of its basis functions, further investigation is needed before attributing any discrepancies to the shortcomings of either model.

Figure 4 shows the magnitude of the helium bulge ratio as a function of height, during solar minimum solstice conditions. These profiles were constructed by taking the ratio of maximum-to-minimum helium number

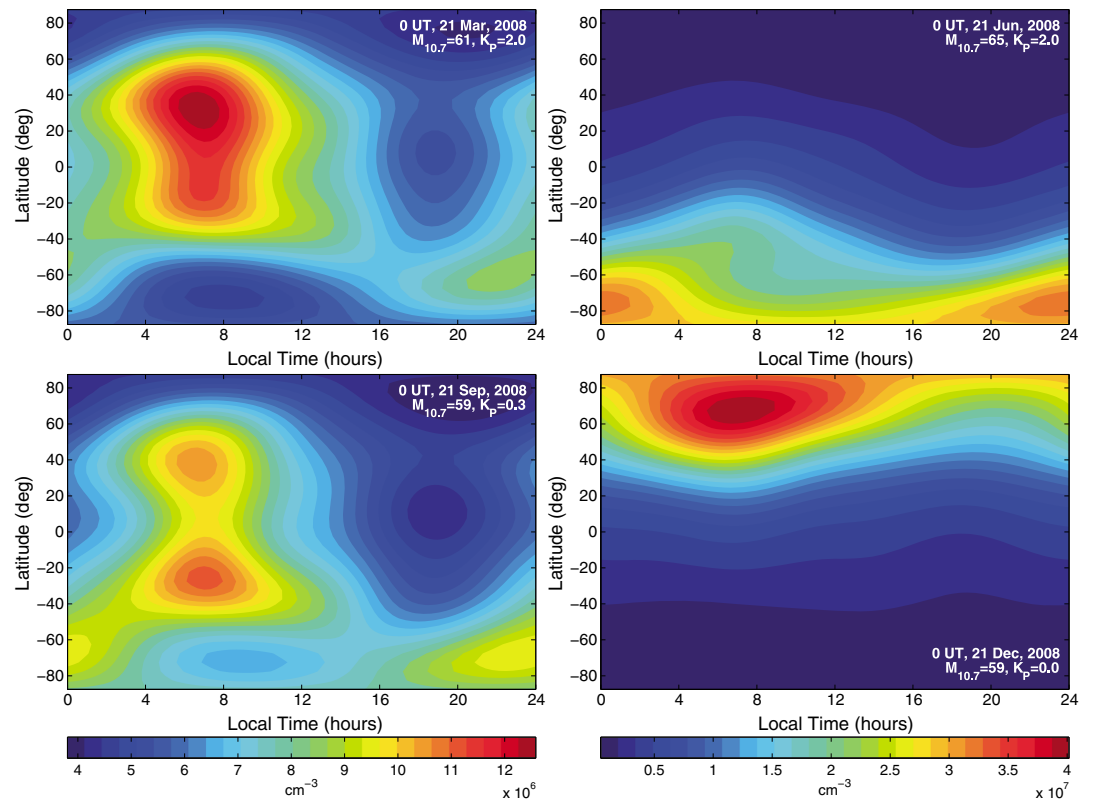


Figure 3. Global distribution of helium number densities at 250 km altitude during each season for solar minimum conditions (2008), as calculated by MSIS. (left) Equinox plots share a common color scale, as do (right) solstice plots; these are distinct from the color scales of Figure 2.

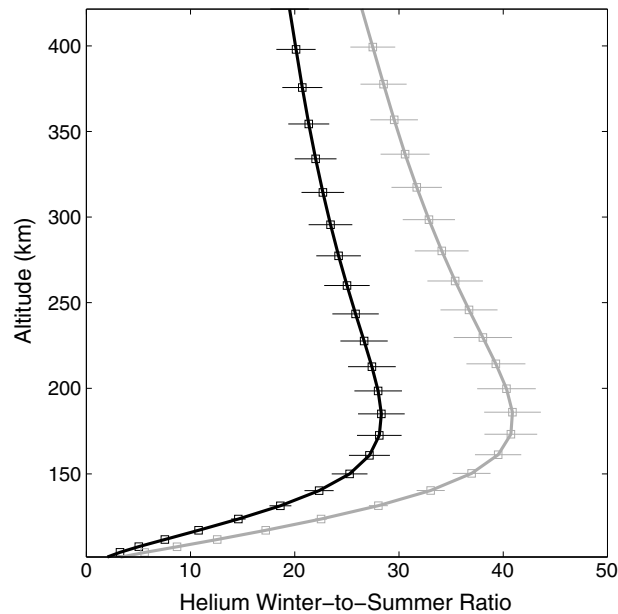


Figure 4. Vertical profile of the winter-to-summer helium bulge ratio during solar minimum June (black, 21 Jun. 2008) and December (grey, 21 Dec. 2008) solstice conditions. The profiles represent the daily average of the ratio of maximum-to-minimum helium number densities taken along each meridian, roughly approximating the sampling of a polar-orbiting satellite (see text for a detailed explanation). Error bars indicate the standard deviation of values over the course of a day.

densities along each model meridian to roughly approximate the method of calculation used in previous studies. The ratio at each height was then averaged both zonally and over the course of a day; note that no attempt was made to specify the local time sampling of a particular polar-orbiting satellite. The vertical profiles exhibit a quick increase from the lower boundary, giving way to a maximum around 175 km and then decaying slowly with altitude to the upper boundary. This behavior can be explained by the transition from a region below the peak which is dominated by collisions to a region above the peak where diffusive equilibrium is well established. Below the height of maximum bulge ratio, the summer-to-winter bulk circulation pattern leads to the accumulation of helium in the winter hemisphere. Above this height, however, vertical profiles begin to approximate diffusive equilibrium, causing helium densities in the winter

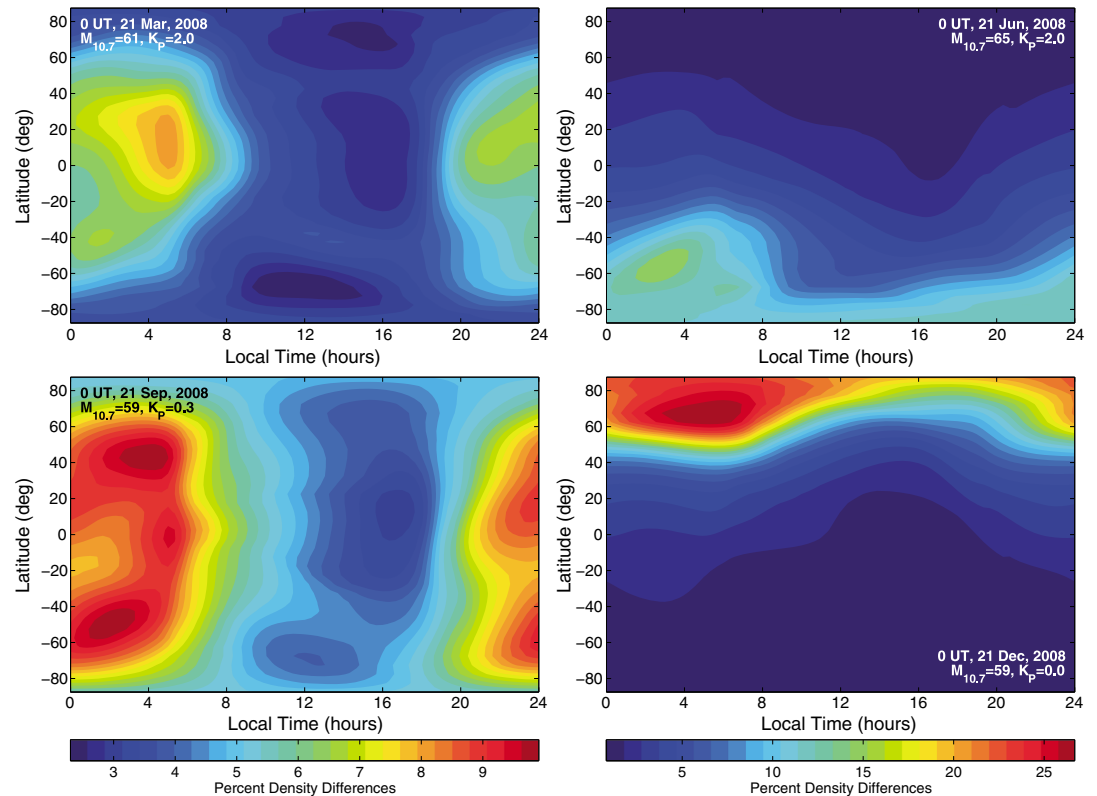


Figure 5. Percent increase in the total mass density at a fixed altitude of 415 km resulting from the inclusion of helium in TIE-GCM during each season for solar minimum conditions (2008). (left) Equinox plots share a common color scale, as do (right) solstice plots.

hemisphere to decrease with height at a slightly faster exponential rate than those in the warmer summer hemisphere.

The significant difference between June and December is due to a combination of lower solar flux and geomagnetic activity during the December solstice. Smaller contributions to this difference may arise from seasonal variations such as in the eddy diffusivity. Error bars in Figure 4 show the standard deviation of the helium ratio over the course of a day, giving an indication of the sensitivity to diurnal variations as well as small variations in geomagnetic activity. Below 150 km, smaller standard deviations are seen, indicating that variations in the lower part of the profile take place on longer timescales. Presumably, the lower portion of the profile is more sensitive to season and solar flux than to short-scale geomagnetic activity. Approaching altitudes as low as 100 km, the two profiles begin to converge, suggesting a muted response to geomagnetic activity as well as to seasonal variations.

The addition of helium to the TIE-GCM has several feedback effects on the global structure of the model. Most of these are related to the change in the mean mass, which can become quite small and even approach 4 amu near the top of the model. On levels of constant pressure, such a decrease in the mean mass corresponds directly to a decrease in mass density. At a fixed height, however, this behavior is accompanied by the expansion of the atmosphere according to the ideal gas law, causing levels of constant pressure to move upward. With increasing altitude, the expansion effect begins to dominate the mean mass effect such that the decay in mass density with height becomes much more gradual when helium is considered. Figure 5 shows the induced increase in mass density at a fixed altitude of 415 km. While the inclusion of helium causes the model's upper boundary to expand considerably higher than 415 km, we chose this height for our comparison because it was the highest altitude that remained within the vertical domain of the original TIE-GCM simulations during each of the four time periods shown.

The increase in mass density is most noticeable during solstice, where differences of 20–25% can be seen. Both equinox and solstice mass density increases are largest under quiet geomagnetic conditions. While

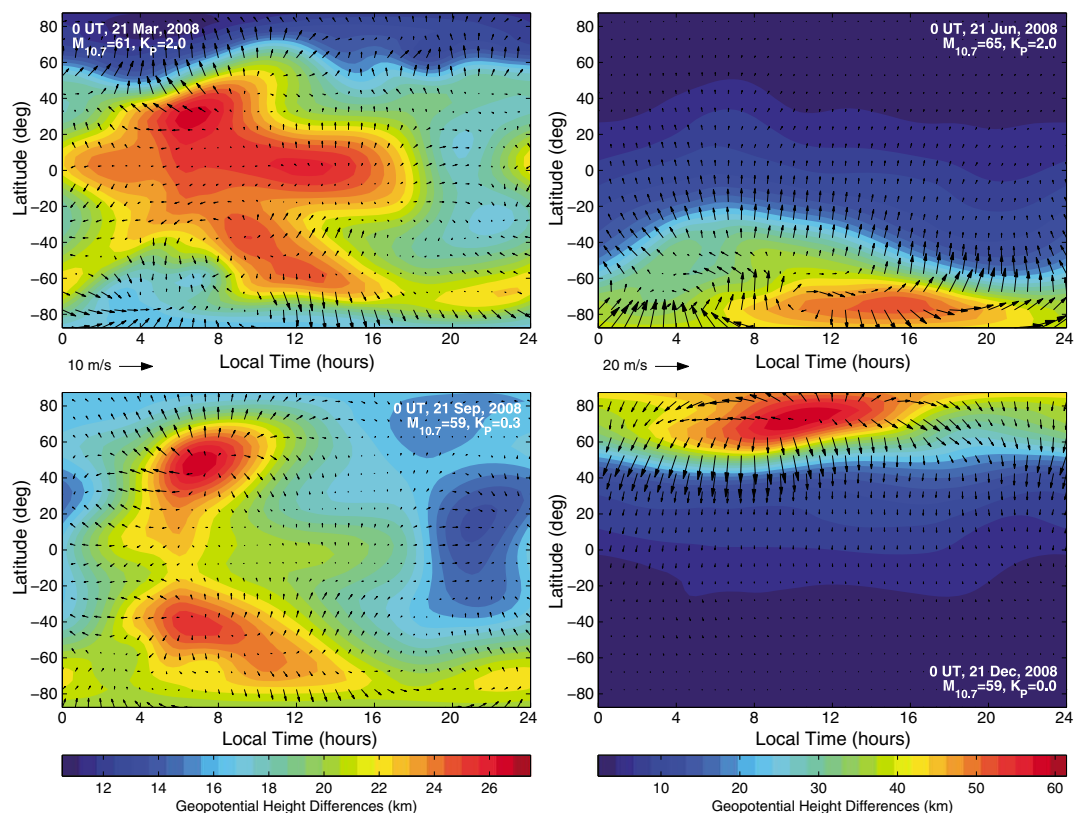


Figure 6. Difference in the geopotential height (color contours) and the horizontal wind field (vectors) on a level of constant pressure near the upper model boundary ($z = +6.75$) resulting from the inclusion of helium in TIE-GCM during each season for solar minimum conditions (2008). (left) Equinox plots share common color and vector scales, as do (right) solstice plots.

somewhat modest, these percent differences increase with height at an approximate rate of 1% per kilometer near the upper boundary of the TIE-GCM in regions of large helium densities. If the composition of the TIE-GCM is extended vertically into the exosphere under the first-order approximation of diffusive equilibrium, the effects of helium soon become the dominant factor in neutral mass density variations. Under solar minimum conditions, an extension of both models to 500 km results in differences on the order of 50% during equinox and 100–200% during solstice. At 600 km, the solstice differences exceed an order of magnitude.

Contours in Figure 6 show differences in the height of a log pressure level near the top of the model induced by the inclusion of helium. Near the winter pole where these height differences maximize, the atmosphere is uplifted by some 50–60 km when compared to an atmosphere simulated without helium. This modification further couples to the horizontal momentum equations [see Dickinson *et al.*, 1981], increasing horizontal gradients in the geopotential and resulting in a difference wind pattern that flows away from the winter helium bulge, as depicted by the vector arrows of Figure 6. This effect generally becomes noticeable in the upper thermosphere, above 300–400 km, where differences as high as 15–20 m/s can be attained.

4. Summary and Conclusions

This paper establishes methods for tracking helium abundance self-consistently throughout the thermosphere. The resulting model simulations qualitatively recreate the expected seasonal/latitudinal behavior while also showing reasonable quantitative agreement with MSIS. Moreover, the model provides winter-to-summer helium ratios that generally agree with solar minimum observations from AE-C [Cageo and Kerr, 1984]. A more rigorous one-to-one comparison between this new model and legacy mass spectrometer measurements is merited; however, this task is left for future work.

Perhaps the most direct application for this new model is related to the increased realism of the neutral mass density vertical profile, and thus the improvement in model performance with respect to satellite drag

observations in the upper thermosphere. At a constant height within the model domain, we have shown that including helium in the TIE-GCM causes differences in neutral mass density on the order of 20–30% during solar minimum. The most noticeable differences occur near the upper model boundary during solstice in the winter hemisphere.

Furthermore, helium concentration in the exosphere is highly sensitive to the dynamics of the thermosphere. An appropriate exospheric model could use the TIE-GCM's upper boundary to specify a realistic exobase. Using profiles approximated by diffusive equilibrium above the TIE-GCM's upper boundary, we demonstrated that helium can account for order-of-magnitude differences in neutral density near 600 km and above. These differences, structured in latitude and local time, are strongly modulated by season and geomagnetic activity, lending significant variability to the upper thermosphere and exosphere. These seasonal, latitudinal, and local time helium behaviors can be used to inform the structure of semiempirical model basis functions [e.g., Sutton *et al.*, 2012]. At a minimum, inferring the amplitude of such basis functions would require sufficient coverage of high-altitude satellite drag measurements but would be better served by a contemporary set of mass spectrometer measurements.

The value of helium as a tracer of thermospheric dynamics has been known for some time [see Reber, 1976]. In addition to its ability to diagnose the interplay of circulation and diffusion in the thermosphere, our new model will enable future studies attempting to exploit the sensitivity of the helium distribution to otherwise unobservable system dynamics and inputs. We anticipate that employing helium as a diagnostic tracer—e.g., in order to specify or constrain high-latitude energy inputs, solar-driven circulation pattern strength, and/or subgrid-scale model dynamics—will be beneficial in refining model performance for scientific endeavors as well as operational applications.

Appendix A: Time-Dependent Thermospheric Composition for N Components

In this section, an equation describing the evolution of major species composition in a log pressure coordinate frame is derived by combining the species-dependent continuity and diffusion equations. The derivation closely follows that of Dickinson and Ridley [1972]; however, additional terms describing time dependence, eddy, and thermal diffusion are included to reflect the current implementation within the TIE-GCM. We also deviate slightly from their treatment to highlight several equations that are useful in tracking species-dependent as well as mass-averaged transport. The following definitions are used:

| | |
|------------------|--|
| D_{ij} | mutual diffusion coefficient of the i th and j th components |
| g | gravitational acceleration |
| H_i | scale height of the i th component [= $kT/(m_i g)$] |
| H | scale height of mixture [= $kT/(\bar{m}g)$] |
| \hat{K}_E, K_E | eddy diffusion coefficients |
| k | Boltzmann constant |
| \mathbf{L} | differential matrix operator of normalized pressure forces |
| m_i | molecular mass of the i th component |
| \bar{m} | mean molecular mass [= $(\sum_{i=1}^N n_i m_i)/n$] |
| n_i | number density of the i th component |
| n | total number density [= $\sum_{i=1}^N n_i$] |
| p_i | partial pressure of the i th component [= $n_i kT$] |
| p_0 | reference pressure |
| p | pressure |
| S_i | source or sink for number density of the i th component |
| \mathbf{s} | vector containing the first $(N - 1)$ components of $m_i S_i / \rho$ |
| T | temperature |
| \mathbf{V} | horizontal component of the momentum-weighted mean velocity |
| \hat{w} | vertical component of the momentum-weighted mean velocity [= $D\hat{z}/Dt$] |
| w_i | deviation of vertical velocity of the i th component from mean velocity |
| w'_i | contribution to w_i from molecular diffusion |
| w''_i | contribution to w_i from eddy diffusion |
| \mathbf{w} | vector containing the first $(N - 1)$ components of $n_i m_i w_i$ |
| \mathbf{w}' | vector containing the first $(N - 1)$ components of $n_i m_i w'_i$ |

- \mathbf{w}'' vector containing the first $(N - 1)$ components of $n_i m_i w_i''$
 \hat{z} vertical spatial coordinate
 z vertical log pressure coordinate [= $\ln(p_0/p)$]
 α diffusion matrix
 α_{Ti} thermal diffusion coefficient of the i th component
 θ latitude
 λ longitude
 v_i volume mixing ratio of the i th component [= n_i/n]
 ρ mass density of mixture [= $\sum_{i=1}^N n_i m_i$]
 ψ_i relative density of i th component [= $n_i m_i / \rho$]
 Ψ vector containing the first $(N - 1)$ components of ψ_i
 ω vertical motion relative to log pressure coordinates [= Dz/Dt]

A1. Mass Continuity

Neglecting horizontal diffusion, each component satisfies the following continuity equation:

$$\frac{\partial}{\partial \hat{z}}(n_i m_i w_i) = m_i S_i - \frac{\partial}{\partial t}(n_i m_i) - \nabla \cdot (n_i m_i \mathbf{V}) - \frac{\partial}{\partial \hat{z}}(n_i m_i \hat{w}) \quad (\text{A1})$$

The right-hand side of (A1) can be written in terms of the relative densities:

$$\frac{\partial}{\partial \hat{z}}(n_i m_i w_i) = m_i S_i - \left(\frac{\partial}{\partial t}(\psi_i \rho) + \nabla \cdot (\psi_i \rho \mathbf{V}) + \frac{\partial}{\partial \hat{z}}(\psi_i \rho \hat{w}) \right) \quad (\text{A2})$$

We wish to transform equation (A2) from a spatial to log pressure vertical coordinate system under the assumption of hydrostatic equilibrium using the following relationship:

$$d\hat{z} = H dz \quad (\text{A3})$$

When applying this transformation to partial derivatives with respect to time and horizontal spatial coordinates, the vertical coordinate being held constant must be considered. The following equations, which also require the assumption of hydrostatic equilibrium, are used to complete this transformation [cf. *Kasahara*, 1974, equations (3.6) and (3.17)]:

$$\left(\frac{\partial}{\partial t} \right)_{\hat{z}} (\psi_i \rho) = \left(\frac{\partial}{\partial t} \right)_z (\psi_i \rho) - \frac{1}{H} \left(\frac{\partial \hat{z}}{\partial t} \right)_z \frac{\partial}{\partial \hat{z}} (\psi_i \rho) \quad (\text{A4})$$

$$\nabla_{\hat{z}} \cdot (\psi_i \rho \mathbf{V}) = \nabla_z \cdot (\psi_i \rho \mathbf{V}) - \frac{1}{H} (\nabla_z \hat{z}) \cdot \frac{\partial}{\partial \hat{z}} (\psi_i \rho \mathbf{V}) \quad (\text{A5})$$

where the subscripts \hat{z} and z refer to the vertical coordinate being held constant under partial differentiation. Additionally, the relationship between the spatial and log pressure vertical velocities is as follows [cf. *Kasahara*, 1974, equation (3.12)]:

$$\hat{w} = \omega H + \left(\frac{\partial \hat{z}}{\partial t} \right)_z + \mathbf{V} \cdot \nabla_z \hat{z} \quad (\text{A6})$$

Making the appropriate substitutions, noting that the equation of state and our assumption of hydrostatic equilibrium imply

$$\rho H = \frac{p_0}{g} e^{-z} \quad (\text{A7})$$

and dropping the subscript z from derivatives taken with respect to time and horizontal spatial coordinates, equation (A2) becomes

$$\frac{\partial}{\partial \hat{z}}(n_i m_i w_i) = -\frac{p_0 e^{-z}}{g} \left(\frac{\partial \psi_i}{\partial t} + \nabla \cdot (\psi_i \mathbf{V}) + e^z \frac{\partial}{\partial \hat{z}} (\psi_i e^{-z} \omega) - \frac{m_i S_i}{\rho} \right) \quad (\text{A8})$$

The definition of w_i implies

$$\sum_{i=1}^N n_i m_i w_i = 0 \quad (\text{A9})$$

Mass sources are assumed to arise solely from the dissociation of one molecule into others so that

$$\sum_{i=1}^N m_i S_i = 0 \quad (\text{A10})$$

Relative densities ψ_i are defined so that

$$\sum_{i=1}^N \psi_i = 1 \quad (\text{A11})$$

By combining (A8) for each component and noting (A9), (A10), and (A11), the continuity equation describing the total fluid in log pressure coordinates is obtained:

$$\nabla \cdot \mathbf{V} + e^z \frac{\partial}{\partial z} (e^{-z} \omega) = 0 \quad (\text{A12})$$

Thus, by invoking the assumption of hydrostatic equilibrium and adopting pressure coordinates, the mass flow of the fluid appears incompressible, transforming the mass continuity equation from a prognostic to diagnostic equation (i.e., no time derivatives appear in the equation).

Using equation (A12), the divergence terms of equation (A8) can be simplified in favor of advection terms, yielding the following equation:

$$\frac{\partial}{\partial z} (n_i m_i w_i) = -\frac{p_0 e^{-z}}{g} \left(\frac{\partial \psi_i}{\partial t} + \mathbf{V} \cdot \nabla \psi_i + \omega \frac{\partial \psi_i}{\partial z} - \frac{m_i S_i}{\rho} \right) \quad (\text{A13})$$

Now let \mathbf{w} be the $(N-1)$ vector with components $m_i n_i w_i$, \mathbf{s} the $(N-1)$ vector with components $m_i S_i / \rho$, and Ψ the $(N-1)$ vector with elements ψ_i . Then the first $(N-1)$ equations of (A13) can be written in vector form as

$$\frac{\partial}{\partial z} \mathbf{w} = -\frac{p_0}{g} e^{-z} \left(\frac{\partial \Psi}{\partial t} + \mathbf{V} \cdot \nabla \Psi + \omega \frac{\partial \Psi}{\partial z} - \mathbf{s} \right) \quad (\text{A14})$$

A2. Molecular and Thermal Diffusion

With the assumption that the atmosphere is in a state of hydrostatic equilibrium, i.e., $\partial p / \partial z = -\rho g$, the equation of motion for the i th component of an N -component mixture in the presence of molecular and thermal diffusion [cf. *Chapman and Cowling*, 1970, equations (18.2,5) and (18.3,13)] can be written:

$$\sum_{j \neq i}^N \frac{n_i n_j}{n D_{ij}} (w'_j - w'_i) = n_i \left(\frac{1}{p_i} \frac{\partial p_i}{\partial z} + \frac{1}{H_i} + \frac{\alpha_{Ti}}{T} \frac{\partial T}{\partial z} \right) \quad (\text{A15})$$

The pressure force exerted on molecules of the i th component, expressed by the right-hand side of (A15), forces these molecules to flow through the rest of the mixture in balance with collisional drags given by the left-hand side.

Noting the partial pressure $p_i = p \psi_i \bar{m} / m_i$, (A15) becomes

$$\frac{1}{n} \sum_{j \neq i}^N \left[\frac{\psi_j}{m_j D_{ij}} (n_j m_j w'_j) - \frac{\psi_i}{m_j D_{ij}} (n_i m_i w'_i) \right] = \left[\frac{\partial}{\partial z} - \left(\frac{1}{H} - \frac{1}{H_i} - \frac{1}{\bar{m}} \frac{\partial \bar{m}}{\partial z} - \frac{\alpha_{Ti}}{T} \frac{\partial T}{\partial z} \right) \right] \psi_i \quad (\text{A16})$$

Equations (A9) and (A11)—noting that the former applies to ticked quantities as well—are now used to eliminate w'_N and ψ_N from the first $(N-1)$ equations of (A16), giving for the i th component

$$\sum_{j=1}^{N-1} \hat{\alpha}_{ij} (m_j n_j w'_j) = \left[\frac{\partial}{\partial z} - \left(\frac{1}{H} - \frac{1}{H_i} - \frac{1}{\bar{m}} \frac{\partial \bar{m}}{\partial z} - \frac{\alpha_{Ti}}{T} \frac{\partial T}{\partial z} \right) \right] \psi_i \quad (\text{A17})$$

where

$$\hat{\alpha}_{ij} = \begin{cases} -\frac{1}{n} \left[\frac{1}{m_N D_{iN}} + \sum_{k \neq i}^{N-1} \left(\frac{1}{m_k D_{ik}} - \frac{1}{m_N D_{iN}} \right) \psi_k \right], & j = i \\ \frac{1}{n} \left(\frac{1}{m_j D_{ij}} - \frac{1}{m_N D_{iN}} \right) \psi_i, & j \neq i \end{cases} \quad (\text{A18})$$

and m_N refers to the molecular mass of the N th species.

Now let $\hat{\alpha}$ be the $(N-1) \times (N-1)$ matrix with elements $\hat{\alpha}_{ij}$ and $\hat{\mathbf{L}}$ the diagonal matrix of differential operators with elements

$$\hat{L}_{ij} = \delta_{ij} \left[\frac{\partial}{\partial \hat{z}} - \left(\frac{1}{H} - \frac{1}{H_i} - \frac{1}{\bar{m}} \frac{\partial \bar{m}}{\partial \hat{z}} - \frac{\alpha_{Ti}}{T} \frac{\partial T}{\partial \hat{z}} \right) \right] \quad (\text{A19})$$

The solution of the nonsingular system of equations (A17) can now be expressed in matrix form:

$$\mathbf{w}' = \hat{\alpha}^{-1} \hat{\mathbf{L}} \Psi \quad (\text{A20})$$

Following *Dickinson and Ridley* [1972], a nondimensional form of the diffusion matrix $\hat{\alpha}$ can be derived using a nondimensional parameter ϕ_{ij} related to the mutual diffusion coefficient through

$$\phi_{ij} = \frac{m_N D}{m_j D_{ij}} \quad (\text{A21})$$

where D is a characteristic diffusion coefficient. It is assumed that D varies with pressure and temperature in the following way:

$$D = D_0 \left(\frac{p_{00}}{p} \right) \left(\frac{T}{T_{00}} \right)^{1.75} \quad (\text{A22})$$

where $D_0 = 0.2$ is the characteristic diffusion coefficient at STP, $T_{00} = 273$ K, $p_{00} = 10^6$ g/(cm \cdot s 2).

The parameter $\hat{\alpha}_{ij}$ defined by equation (A18) is nondimensionalized by the substitution

$$\alpha_{ij} = (m_N n D) \hat{\alpha}_{ij} \quad (\text{A23})$$

where the nondimensional parameter α_{ij} is then

$$\alpha_{ij} = \begin{cases} - \left[\phi_{iN} + \sum_{k \neq i}^{N-1} (\phi_{ik} - \phi_{iN}) \psi_k \right], & j = i \\ (\phi_{ij} - \phi_{iN}) \psi_i, & j \neq i \end{cases} \quad (\text{A24})$$

Additionally, equations (A3) and (A7) are again used to transform the vertical coordinate of the right-hand side of equation (A20) into log pressure levels, resulting in

$$\mathbf{w}' = \tau^{-1} \left(\frac{T_{00}}{T} \right)^{0.25} \frac{p_0 \bar{m}}{m_N g} \alpha^{-1} \mathbf{L} \Psi \quad (\text{A25})$$

where

$$L_{ij} = \delta_{ij} \left[\frac{\partial}{\partial z} - \left(1 - \frac{m_i}{\bar{m}} - \frac{1}{\bar{m}} \frac{\partial \bar{m}}{\partial z} - \frac{\alpha_{Ti}}{T} \frac{\partial T}{\partial z} \right) \right] \quad (\text{A26})$$

τ is a characteristic diffusion timescale defined by

$$\tau = \frac{p_0}{p_{00}} \frac{H_0^2}{D_0} \quad (\text{A27})$$

and H_0 is a characteristic scale height:

$$H_0 = \frac{k T_{00}}{m_N g} \quad (\text{A28})$$

A3. Eddy Diffusion

In an atmosphere dominated by a single constituent, as is the case with molecular nitrogen in the lower thermosphere, eddy diffusion establishes a flow which acts to smooth gradients in the volume mixing ratio of the minor constituents, v_i , as follows [*Lettau*, 1951; *Colegrove et al.*, 1965]:

$$w_i'' = -\hat{K}_E \frac{1}{v_i} \frac{\partial v_i}{\partial \hat{z}} \quad (\text{A29})$$

In terms of mass flow rates and mixing ratios, equation (A29) becomes

$$n_i m_i w_i'' = -n \bar{m} \hat{K}_E \left(\frac{\partial}{\partial \hat{z}} + \frac{1}{\bar{m}} \frac{\partial \bar{m}}{\partial \hat{z}} \right) \psi_i \quad (\text{A30})$$

Transforming to log pressure coordinates and writing in vector form, equation (A30) becomes

$$\mathbf{w}'' = -\frac{p_0}{g} K_E e^{-z} \left(\frac{\partial}{\partial z} + \frac{1}{\bar{m}} \frac{\partial \bar{m}}{\partial z} \right) \Psi \quad (\text{A31})$$

where $K_E \equiv \hat{K}_E / H^2$.

A4. Composition Equation

Setting the total species-dependent mass flux $\mathbf{w} = \mathbf{w}' + \mathbf{w}''$ and combining equations (A25) and (A31) to eliminate \mathbf{w} from equation (A14) yield the composition equation

$$\frac{\partial}{\partial z} \left[\tau^{-1} \left(\frac{T_{00}}{T} \right)^{0.25} \frac{\bar{m}}{m_N} \alpha^{-1} \mathbf{L}\Psi - K_E e^{-z} \left(\frac{\partial}{\partial z} + \frac{1}{\bar{m}} \frac{\partial \bar{m}}{\partial z} \right) \Psi \right] = e^{-z} \left(\mathbf{s} - \frac{\partial \Psi}{\partial t} - \mathbf{v} \cdot \nabla \Psi - \omega \frac{\partial \Psi}{\partial z} \right) \quad (\text{A32})$$

In the current TIE-GCM implementation, the subscripting order of the major neutral species is as follows: $i = \{\text{O}_2, \text{O}, \text{He}\}$, with N_2 chosen to be the N th species due in part to the assumptions stated in section A3.

Acknowledgments

The authors gratefully acknowledge E.C. Ridley, whose detailed notes regarding the solution of helium as a minor species are maintained by A. Maute of NCAR/HAO. Model simulations and data used throughout this article are freely available by request from E.S. This work is supported by AFOSR grant LRIR 13RV09COR to the Air Force Research Laboratory, NASA grants NNX10AQ52G and NNX10AE62G to the University of Colorado, and NASA grants NNX13AE15G and NNX10AQ59G to the National Center for Atmospheric Research. NCAR is sponsored by the National Science Foundation.

Larry Kepko thanks two anonymous reviewers for assistance in evaluating this manuscript.

References

- Banks, P. M., and G. Kockarts (1973), *Aeronomy: Part B*, Academic Press, New York.
- Cageao, R. P., and R. B. Kerr (1984), Global distribution of helium in the upper atmosphere during solar minimum, *Planet. Space Sci.*, **32**, 1523–1529, doi:10.1016/0032-0633(84)90019-9.
- Chapman, S., and T. G. Cowling (1970), *The Mathematical Theory of Non-uniform Gases*, 3rd ed.
- Colegrove, F. D., W. B. Hanson, and F. S. Johnson (1965), Eddy diffusion and oxygen transport in the lower thermosphere, *J. Geophys. Res.*, **70**, 4931–4941, doi:10.1029/JZ070i019p04931.
- Colegrove, F. D., F. S. Johnson, and W. B. Hanson (1966), Atmospheric composition in the lower thermosphere, *J. Geophys. Res.*, **71**, 2227–2236, doi:10.1029/JZ071i009p02227.
- Cook, G. E. (1967), The large semi-annual variation in exospheric density: A possible explanation, *Planet. Space Sci.*, **15**, 627–632, doi:10.1016/0032-0633(67)90036-0.
- Dickinson, R. E., and E. C. Ridley (1972), Numerical solution for the composition of a thermosphere in the presence of a steady subsolar-to-antisolar circulation with application to Venus, *J. Atmos. Sci.*, **29**, 1557–1570, doi:10.1175/1520-0469(1972)029<1557:NSFTCO>2.0.CO;2.
- Dickinson, R. E., E. C. Ridley, and R. G. Roble (1981), A three-dimensional general circulation model of the thermosphere, *J. Geophys. Res.*, **86**, 1499–1512, doi:10.1029/JA086iA03p01499.
- Dickinson, R. E., E. C. Ridley, and R. G. Roble (1984), Thermospheric general circulation with coupled dynamics and composition, *J. Atmos. Sci.*, **41**, 205–219, doi:10.1175/1520-0469(1984)041<0205:TGCWCD>2.0.CO;2.
- Hagan, M. E., R. G. Roble, and J. Hackney (2001), Migrating thermospheric tides, *J. Geophys. Res.*, **106**, 12,739–12,752, doi:10.1029/2000JA000344.
- Hays, P. B., R. A. Jones, and M. H. Rees (1973), Auroral heating and the composition of the neutral atmosphere, *Planet. Space Sci.*, **21**, 559–573, doi:10.1016/0032-0633(73)90070-6.
- Hedin, A. E. (1987), MSIS-86 thermospheric model, *J. Geophys. Res.*, **92**, 4649–4662, doi:10.1029/JA092iA05p04649.
- Hedin, A. E. (1991), Extension of the MSIS thermosphere model into the middle and lower atmosphere, *J. Geophys. Res.*, **96**, 1159–1172, doi:10.1029/90JA02125.
- Hedin, A. E., and G. R. Carignan (1985), Morphology of thermospheric composition variations in the quiet polar thermosphere from Dynamics Explorer measurements, *J. Geophys. Res.*, **90**, 5269–5277, doi:10.1029/JA090iA06p05269.
- Hedin, A. E., H. G. Mayr, C. A. Reber, N. W. Spencer, and G. R. Carignan (1974), Empirical model of global thermospheric temperature and composition based on data from the Ogo 6 quadrupole mass spectrometer, *J. Geophys. Res.*, **79**, 215–225, doi:10.1029/JA079i001p00215.
- Heelis, R. A., J. K. Lowell, and R. W. Spiro (1982), A model of the high-latitude ionospheric convection pattern, *J. Geophys. Res.*, **87**, 6339–6345, doi:10.1029/JA087iA08p06339.
- Hodges, R. R. Jr. (1970), Vertical transport of minor constituents in the lower thermosphere by nonlinear processes of gravity waves, *J. Geophys. Res.*, **75**, 4842–4848, doi:10.1029/JA075i025p04842.
- Hodges, R. R. Jr. (1973), Differential equation of exospheric lateral transport and its application to terrestrial hydrogen, *J. Geophys. Res.*, **78**, 7340–7346, doi:10.1029/JA078i031p07340.
- Hodges, R. R. Jr., and F. S. Johnson (1968), Lateral transport in planetary exospheres, *J. Geophys. Res.*, **73**, 7307–7317, doi:10.1029/JA073i023p07307.
- Johnson, F. S., and B. Gottlieb (1970), Eddy mixing and circulation at ionospheric levels, *Planet. Space Sci.*, **18**, 1707–1718, doi:10.1016/0032-0633(70)90004-8.
- Kasahara, A. (1974), Various vertical coordinate systems used for numerical weather prediction, *Mon. Weather Rev.*, **102**, 509–522, doi:10.1175/1520-0493(1974)102<0509:VVCSUF>2.0.CO;2.
- Kasprzak, W. T. (1969), Evidence for a helium flux in the lower thermosphere, *J. Geophys. Res.*, **74**, 894–896, doi:10.1029/JA074i003p00894.
- Keating, G. M., and E. J. Prior (1968), The winter helium bulge, in *Space Research VIII; Proceedings Of The Tenth Cospar Plenary Meeting, Imperial Coll. of Science and Technology, London, England, Jul. 24–29, 1967*, edited by A. P. Mitra, L. G. Jacchia, and W. S. Newman, pp. 982–992, North-Holland, Amsterdam.
- Keating, G. M., J. A. Mullins, and E. J. Prior (1970), The polar exosphere near solar maximum, in *Space Research X; Proceedings of Twelfth Planetary Meeting of Cospar, Prague, Czechoslovakia, May 1969*, edited by T. M. Donahue, P. A. Smith, and L. Thomas, pp. 439–449, North-Holland, Amsterdam.
- Keating, G. M., E. J. Prior, D. S. McDougal, and J. I. Nicholson (1974), A critical evaluation of the OGO 6 helium model, in *Space Research XV; Proceedings of 17th Annual Cospar Meeting, Comm. on Space Res., Sao Paulo, Brazil*, edited by M. J. Rycroft, pp. 273–278, North-Holland, Amsterdam.
- Keeling, C. D., and T. P. Whorf (2005), Atmospheric CO₂ records from sites in the SIO air sampling network, in *Trends: A Compendium of Data on Global Change*, Carbon Dioxide Information Analysis Center, Oak Ridge Natl. Lab., U.S. Dep. of Energy, Oak Ridge, Tenn., doi:10.3334/CDIAC/atg.035.
- Kockarts, G. (1972), Distribution of hydrogen and helium in the upper atmosphere, *J. Atmos. Terr. Phys.*, **34**, 1729–1743, doi:10.1016/0021-9169(72)90032-3.
- Kockarts, G. (1973), Helium in the terrestrial atmosphere, *Space Sci. Rev.*, **14**, 723–757, doi:10.1007/BF00224775.
- Lettau, H. (1951), Diffusion in the upper atmosphere, in *Compendium of Meteorology*, edited by T. F. Malone, pp. 320–333, Am. Meteorol. Soc., New York.

- Liu, X., J. P. Thayer, A. Burns, W. Wang, and E. K. Sutton (2014a), Altitude variations in the thermosphere mass density response to geomagnetic activity during the recent solar minimum, *J. Geophys. Res. Space Physics*, *119*, 2160–2177, doi:10.1002/2013JA019453.
- Liu, X., W. Wang, J. P. Thayer, A. Burns, E. K. Sutton, S. C. Solomon, L. Qian, and G. Lucas (2014b), The winter helium bulge revisited, *Geophys. Res. Lett.*, *41*, 6603–6609, doi:10.1002/2014GL061471.
- Mauersberger, K., D. C. Kayser, W. E. Potter, and A. O. Nier (1976a), Seasonal variation of neutral thermospheric constituents in the Northern Hemisphere, *J. Geophys. Res.*, *81*, 7–11, doi:10.1029/JA081i001p00007.
- Mauersberger, K., W. E. Potter, and D. C. Kayser (1976b), A direct measurement of the winter helium bulge, *Geophys. Res. Lett.*, *3*, 269–271, doi:10.1029/GL003i005p00269.
- Mayr, H. G., and H. Volland (1972), Theoretical model for the latitude dependence of the thermospheric annual and semiannual variations, *J. Geophys. Res.*, *77*, 6774–6790, doi:10.1029/JA077i034p06774.
- Mayr, H. G., and H. Volland (1973), A two-component model of the diurnal variations in the thermospheric composition, *J. Atmos. Terr. Phys.*, *35*, 669–680, doi:10.1016/0021-9169(73)90198-0.
- Mayr, H. G., A. E. Hedin, C. A. Reber, and G. R. Carignan (1974), Global characteristics in the diurnal variations of the thermospheric temperature and composition, *J. Geophys. Res.*, *79*, 619–628, doi:10.1029/JA079i004p00619.
- Mayr, H. G., I. Harris, and N. W. Spencer (1978), Some properties of upper atmosphere dynamics, *Rev. Geophys. Space Phys.*, *16*, 539–565, doi:10.1029/RG016i004p00539.
- Newton, G. P., D. T. Pelz, and W. T. Kasprzak (1973), Equatorial thermospheric composition and its variations, in *Space Research XIII; Proceedings of the Fifteenth Plenary Meeting, Madrid, Spain, May 10–24, 1972*, edited by M. J. Rycroft and S. K. Runcorn, pp. 287–290, Akademie-Verlag GmbH, Berlin, East Germany.
- Nicolet, M. (1961), Helium, an important constituent in the lower exosphere, *J. Geophys. Res.*, *66*, 2263–2264, doi:10.1029/JZ066i007p02263.
- Picone, J. M., A. E. Hedin, D. P. Drob, and A. C. Aikin (2002), NRLMSISE-00 empirical model of the atmosphere: Statistical comparisons and scientific issues, *J. Geophys. Res.*, *107*(A12), 1468, doi:10.1029/2002JA009430.
- Qian, L., S. C. Solomon, and T. J. Kane (2009), Seasonal variation of thermospheric density and composition, *J. Geophys. Res.*, *114*, A01312, doi:10.1029/2008JA013643.
- Qian, L., A. G. Burns, S. C. Solomon, and W. Wang (2013), Annual/semiannual variation of the ionosphere, *Geophys. Res. Lett.*, *40*, 1928–1933, doi:10.1002/grl.50448.
- Reber, C. A. (1976), Dynamical effects in the distribution of helium in the thermosphere, *J. Atmos. Terr. Phys.*, *38*, 829–840, doi:10.1016/0021-9169(76)90023-4.
- Reber, C. A., and P. B. Hays (1973), Thermospheric wind effects on the distribution of helium and argon in the Earth's upper atmosphere, *J. Geophys. Res.*, *78*, 2977–2991, doi:10.1029/JA078i016p02977.
- Reber, C. A., and M. Nicolet (1965), Investigation of the major constituents of the April-May 1963 heterosphere by the Explorer XVII satellite, *Planet. Space Sci.*, *13*, 617–646, doi:10.1016/0032-0633(65)90043-7.
- Reber, C. A., D. N. Harpold, R. Horowitz, and A. E. Hedin (1971), Horizontal distribution of helium in the Earth's upper atmosphere, *J. Geophys. Res.*, *76*, 1845–1848, doi:10.1029/JA076i007p01845.
- Reber, C. A., A. E. Hedin, and S. Chandra (1973), Equatorial phenomena in neutral thermospheric composition, *J. Atmos. Terr. Phys.*, *35*, 1223–1228, doi:10.1016/0021-9169(73)90019-6.
- Reber, C. A., A. E. Hedin, D. T. Pelz, L. H. Brace, and W. E. Potter (1975), Phase and amplitude relationships of wave structure observed in the lower thermosphere, *J. Geophys. Res.*, *80*, 4576–4580, doi:10.1029/JA080i034p04576.
- Richards, P. G., J. A. Fennelly, and D. G. Torr (1994), EUVAC: A solar EUV flux model for aeronomic calculations, *J. Geophys. Res.*, *99*, 8981–8992, doi:10.1029/94JA00518.
- Richmond, A. D., E. C. Ridley, and R. G. Roble (1992), A thermosphere/ionosphere general circulation model with coupled electrodynamics, *Geophys. Res. Lett.*, *19*, 601–604, doi:10.1029/92GL00401.
- Roble, R. G., and E. C. Ridley (1987), An auroral model for the NCAR thermospheric general circulation model (TGCM), *Ann. Geophys.*, *5*, 369–382.
- Roble, R. G., and E. C. Ridley (1994), A thermosphere-ionosphere-mesosphere-electrodynamics general circulation model (time-GCM): Equinox solar cycle minimum simulations (30–500 km), *Geophys. Res. Lett.*, *21*, 417–420, doi:10.1029/93GL03391.
- Roble, R. G., E. C. Ridley, A. D. Richmond, and R. E. Dickinson (1988), A coupled thermosphere/ionosphere general circulation model, *Geophys. Res. Lett.*, *15*, 1325–1328, doi:10.1029/GL015i012p01325.
- Schunk, R. W., and A. F. Nagy (2004), *Ionospheres, Cambridge Atmos. and Space Sci. Ser.*, Cambridge Univ. Press, Cambridge, U. K.
- Solomon, S. C., and L. Qian (2005), Solar extreme-ultraviolet irradiance for general circulation models, *J. Geophys. Res.*, *110*, A10306, doi:10.1029/2005JA011160.
- Solomon, S. C., L. Qian, L. V. Didkovsky, R. A. Viereck, and T. N. Woods (2011), Causes of low thermospheric density during the 2007–2009 solar minimum, *J. Geophys. Res.*, *116*, A00H07, doi:10.1029/2011JA016508.
- Solomon, S. C., A. G. Burns, B. A. Emery, M. G. Mlynczak, L. Qian, W. Wang, D. R. Weimer, and M. Wiltberger (2012), Modeling studies of the impact of high-speed streams and co-rotating interaction regions on the thermosphere-ionosphere, *J. Geophys. Res.*, *117*, A00L11, doi:10.1029/2011JA017417.
- Sutton, E. K. (2011), Accelerometer-derived atmospheric density from the CHAMP and GRACE satellites, *AFRL Tech. Rep., DTIC# ADA537198*, Defense Technical Information Center (DTIC), Fort Belvoir, Va. [Available at <http://www.dtic.mil/docs/citations/ADA537198> and <http://www.dtic.mil/dtic/tr/fulltext/u2/a537198.pdf>].
- Sutton, E. K., S. B. Cable, C. S. Lin, L. Qian, and D. R. Weimer (2012), Thermospheric basis functions for improved dynamic calibration of semi-empirical models, *Space Weather*, *10*, S10001, doi:10.1029/2012SW000827.
- Swarztrauber, P. (1979), On the spectral approximation of discrete scalar and vector functions on the sphere, *SIAM J. Numer. Anal.*, *16*(6), 934–949, doi:10.1137/0716069.
- Thayer, J. P., X. Liu, J. Lei, M. Pilinski, and A. G. Burns (2012), The impact of helium on thermosphere mass density response to geomagnetic activity during the recent solar minimum, *J. Geophys. Res.*, *117*, A07315, doi:10.1029/2012JA017832.
- Viereck, R. A., L. E. Floyd, P. C. Crane, T. N. Woods, B. G. Knapp, G. Rottman, M. Weber, L. C. Puga, and M. T. Deland (2004), A composite Mg II index spanning from 1978 to 2003, *Space Weather*, *2*, 10005, doi:10.1029/2004SW000084.
- Woods, T. N., and G. J. Rottman (2002), Solar ultraviolet variability over time periods of aeronomic interest, in *Atmospheres in the Solar System: Comparative Aeronomy, Geophys. Monogr. Ser.*, vol. 130, edited by M. Mendillo, A. Nagy, and J. H. Waite, pp. 221–234, AGU, Washington, D. C.
- Zhang, Y., and L. J. Paxton (2008), An empirical *Kp*-dependent global auroral model based on TIMED/GUVI FUV data, *J. Atmos. Sol. Terr. Phys.*, *70*, 1231–1242, doi:10.1016/j.jastp.2008.03.008.